



PDEs on Graphs for Image Reconstruction on Positron Emission Tomography

Abdelwahhab Boudjelal^{1,2(✉)}, Abderrahim Elmoataz¹, François Lozes¹,
and Zoubeida Messali²

¹ Image Team, University of Caen Normandy and the ENSICAEN in the GREYC Laboratory, 6 Boulevard Maréchal Juin, 14050 Caen Cedex, France

{[abdelwahhab.boudjelal](mailto:abdelwahhab.boudjelal@unicaen.fr), [abderrahim.elmoataz](mailto:abderrahim.elmoataz@unicaen.fr), [francois.lozes](mailto:francois.lozes@unicaen.fr)}@unicaen.fr

² Electrical Engineering Laboratory LGE, M'sila University, M'sila, Algeria
messalizoubeida@gmail.com

Abstract. A better quality of an image can be achieved through iterative image reconstruction for positron emission tomography (PET) as it employs spatial regularization that minimizes the difference of image intensity among adjacent pixels. In our previous works, we have proposed a simple method to solve PDEs on general images using the framework of PdEs (Partial difference Equations) on graphs. In this paper, we propose to apply morphological-based operators on graphs for processing of 2D PET images. We apply this approach for to remove noise from the raw projections data. The quality measurements and visual inspections show a significant improvement in image quality compared to conventional Algebraic Reconstruction Technique (ART).

Keywords: Image reconstruction · PET · Post-reconstruction
ART algorithm · PdE framework

1 Introduction

The goal of positron emission tomography (PET) [1], is to provide molecular information on the biology of many diseases inside the human body. Significant advances are also taking place, both in instrumentation for data collection and in computer methods for generating images from measured data. These methods are developed to resolve the inverse problem known as “reconstructing the image from the projections”. However, in the case of limited views (low-dose imaging) and/or limited angle (specific installation constraints), the data available for inversion are not complete, the problem becomes more ill-conditioned and the results Show significant artifacts. In these situations, an alternative approach of reconstruction, based on a discrete model of the problem, consists in using an iterative algorithm or a statistical medialization of the problem to compute an estimate of the unknown object.

Typically, individual projections are distorted during data collection because of noise due to low dose, which originates from the low energy positron due to the positron decay. Positron Emission Tomography (PET) reconstruction are usually ill-posed inverse problems and encounter significant amounts of noise [2,3]. Traditional scanners generally use a reconstructive approach based on analytical filtered back-projection (FBP) that malfunctions in low-data situations and weak signal-to-noise ratios [4]. The use of iterative image reconstruction algorithms [5–8] can circumvent all these shortcomings. The most widely used iterative algorithms in PET are the ML-EM (maximum-likelihood expectation maximization) algorithm and its accelerated version OSEM (Ordered Subset EM). The ML-EM method was introduced by Dempster et al. in 1977 [9] and first applied to PET by Shepp and Vardi [10]. The algebraic reconstruction Technique (ART) [11], considered as an important class of iterative approaches, assume that the cross-sectional section consists of a set of unknown, and then establishes algebraic equations for the unknown in terms of measured projection data.

In this paper, we adopt the PdE framework, and we focus on some PDEs-based continuous morphological operators in the Euclidean domain: dilation/erosion and mean curvature flows. Our motivation is to extend their applications for the processing of 2D PET images. We apply this approach for to remove noise from the raw projections data. The proposed approach is general in the sense that it is independent of the method of reconstruction. As the experiments show, our approach tends to improve the quality of several standard tomographic reconstruction algorithms.

This paper is organized as follows: in Sect. 2, we present acquisition and reconstruction methods. In Sect. 3, we present the proposed reconstruction algorithm. Numerical examples are given in Sect. 4, where we present our reconstruction results and compare the performance with other methods. Finally, the last section concludes.

2 Acquisition and Reconstruction Methods

2.1 The PET Imaging Model

The reconstruction from projections of PET images is a particularity of the general inverse problem of estimating the radioactive activity map related to a measurement p by:

$$p_i = A_{i,j}x_j + n_i \quad (1)$$

In the process of PET imaging reconstruction, x is the reconstructed image, p is the measurement of projection data, A is the system matrix whose component $A_{i,j}$ accounts for the probability of a photon emitted from pixel j being recorded into bin i and n_i is the random and scatter events that add a bias to each detector.

2.2 Algebraic Reconstruction Technique (ART)

The ART is sequential method, i.e., each equation is treated at a time, since each equation is dependent on the previous. The equation of ART [11] is given by

$$x_j^{(k+1)} = x_j^{(k)} + \alpha \frac{p_i - \sum_{n=1}^N A_{i,n} x_n^{(k+1)}}{\sum_{n=1}^N A_{i,n}^2} A_{i,j} \tag{2}$$

where $x_j^{(k+1)}$ and $x_j^{(k)}$ are the current and the new estimates, respectively; $\sum_{n=1}^N A_{i,n} x_n^{(k+1)}$ is the sum weighted pixels along ray i ; for the k^{th} iteration; p_i is the measured projection for the i^{th} ray, and α is the relaxation parameter. The second term on the left in Eq. (2), is the term of correction. The process starts by making an intialguess. Observing Eq. (2), we see that (a) this correction term is added to the current estimate in order to found the new estimate and (b) the comparison consists in the subtraction of the estimated projections from the measured projections. Also, we can easily see, that Eq. (2) is used to update the value of the j^{th} pixel on every ray equation.

3 PDEs on Weighted Graphs for Images and Point Clouds

In this section we recall the PdE method [12]. This latter method enables us to transcribe, for images and point clouds, many PDEs models and algorithms designed for image processing. First, from a point cloud or an image, we construct a local or non-local graph. Then we use the framework of PdE method, that defined discrete difference operators on graph.

3.1 Graph Construction

Considering a surface or a point cloud composed by a set of vertices, such as $S = \{x_1, x_2, \dots\}$. with $x_i \in \mathbb{R}^3$. To each raw point $x_i \in S$, one associates a vertex of a graph G to defined a set of a set of vertices V . Data on image or point cloud can be defined as a function $f : V \rightarrow \mathbb{R}$. The construction of such a graph consists in modeling the neighborhood relationships between the data through the definition of a set of edges E and using a pairwise distance measure $\mu : V \times V \rightarrow \mathbb{R}^+$. In the particular case of images, edges based on geometric neighborhoods are particularly well-adapted to represent the geometry.

The similarity between two vertices is computed by a similarity measure $s : E \rightarrow \mathbb{R}^+$, which satisfies:

$$w(u, v) = \begin{cases} s(u, v), & \text{if } (u, v) \in E \\ 0, & \text{otherwise} \end{cases} \tag{3}$$

Common similarity functions are the following:

$$\begin{cases} s_0(u, v) \equiv 1, \\ s_1(u, v) = \exp\left(-\mu(f^0(u), f^0(v))/\sigma^2\right), \end{cases} \tag{4}$$

for which the variance parameter $\sigma > 0$ usually depends on the variation of the function μ .

The function f used to describe the data at a node u can be considered as a feature vector. Several choices can be considered for the expression of the feature vectors, depending on the nature of the features to be used for graph processing. In the context of image processing one can use a simple gray scale or color feature vector F_u , or a patch feature vector $F_u^\tau = \bigcup_{v \in \mathcal{W}^\tau(u)} F_v$ (i.e, the set of values F_v for which v is in a square window $\mathcal{W}^\tau(u)$ of size $(2\tau + 1) \times (2\tau + 1)$ centered at a vertex pixel u). Note that the latter vector allows to incorporate nonlocal features for $\tau \geq 1$. Therefore, we need a new definition of patches that can be used with any graph representation associated to meshes or point clouds.

3.2 Partial Difference Operators on Graphs

In this subsection, we recall definitions and operators on graphs. This constitutes the basis of the framework of PdEs on a graph [12] that enables to transpose PDEs on graphs.

Notations and Preliminaries. A weighted graph $G = (V, E, w)$ consists of a finite set $V = \{v_1, \dots, v_N\}$ of N vertices and a finite set $E \subset V \times V$ of weighted edges. We assume G to be undirected, with no self-loops and no multiple edges. Let (v_i, v_j) be the edge of E that connects two vertices v_i and v_j of V . Its weight, denoted by $w(v_i, v_j)$, represents the similarity between its vertices. Similarities are usually computed by using a positive symmetric function $w : V \times V \rightarrow \mathbb{R}^+$ satisfying $w(v_i, v_j) = 0$ if $(v_i, v_j) \notin E$. The notation $v_i \sim v_j$ is also used to denote two adjacent vertices. The degree of a vertex v_i is defined as $\delta_w(v_i) = \sum_{v_j \sim v_i} w(v_i, v_j)$. Let $H(V)$ be the Hilbert space of real-valued functions defined on the vertices of a graph. A function $f : V \rightarrow \mathbb{R}$ of $H(V)$ assigns a real value $f(v_i)$ to each vertex $v_i \in V$. $H(V)$ space is endowed with the usual inner products.

Difference Operators on Weighted Graphs. Let $G = (V, E, w)$ be a weighted graph, $f : V \rightarrow \mathbb{R}$ be a function of $H(V)$ and $w : V \times V \rightarrow \mathbb{R}^+$, a weight function that depends on the interactions between the vertices. The *difference operator* [12] of f , noted $d_w : H(V) \rightarrow H(E)$, is defined on an edge $(v_i, v_j) \in E$ by:

$$(d_w f)(v_i, v_j) = \sqrt{w(v_i, v_j)}(f(v_j) - f(v_i)). \tag{5}$$

The *directional derivative* (or *edge derivative* of f , at a vertex $v_i \in V$, along an edge $e = (v_i, v_j)$, is defined as:

$$\partial_{v_j} f(v_i) = (d_w f)(v_i, v_j). \tag{6}$$

The external and internal *morphological directional partial derivative* operators are respectively defined as [13]:

$$\partial^\pm v_j f(v_i) = (\partial_{v_j} f(v_i))^\pm. \tag{7}$$

where $(x)^+ = \max(x, 0)$ and $(x)^- = -\min(x, 0)$.

Discrete upwind non-local weighted gradients are defined as:

$$(\nabla_w^\pm f)(v_i) = \left((\partial_{v_j}^\pm f)(v_i) \right)_{v_j \in V}^T. \tag{8}$$

The \mathcal{L}_p norms and the \mathcal{L}_∞ of these gradients are defined by:

$$\|(\nabla_w^\pm f)(v_i)\|_p = \left[\sum_{v_j \sim v_i} w^p(v_i, v_j) [(f(v_j) - f(v_i))^\pm]^p \right]^{\frac{1}{p}} \tag{9}$$

$$\|(\nabla_w^\pm f)(v_i)\|_\infty = \max_{v_j \sim v_i} (w(v_i, v_j) |(f(v_j) - f(v_i))^\pm|). \tag{10}$$

∇^\pm refers to both external and internal gradients (with respect to the sign). The mean curvature \mathcal{K}_w of a function f at $u \in V$ on a graph is defined as:

$$\mathcal{K}_w(u, f) = \frac{\sum_{f(v)-f(u) \geq 0} w(u, v) - \sum_{f(v)-f(u) < 0} w(u, v)}{\delta_w(u)}. \tag{11}$$

3.3 Regularization Using Mean Curvature Flows on Graphs

In this section we consider a first transposition of PDEs on graphs and propose a methodology to regularize functions defined on the vertices of graphs.

Let $f^0 \in H(V)$ be a given function defined on the vertices of a weighted graph $G = (V, E, w)$. In a given context this function represents an observation of a clean function $h \in H(V)$ corrupted by an additive noise $n \in H(V)$. A common approach is to regularize f^0 by morphological-based algorithms such as the mean curvature flows.

The continuous mean curvature flow equation is formulated as:

$$\frac{\partial \phi}{\partial t} = \text{div} \left(\frac{\nabla \phi}{|\nabla \phi|} \right) |\nabla \phi|, \tag{12}$$

we propose to replace the continuous curvature by the curvature on the graph and to use the following morphological scheme:

$$\begin{cases} \frac{\partial f}{\partial t}(u) = (\mathcal{K}_w(u, f))^+ \|(\nabla_w^+ f)(u)\|_\infty - (\mathcal{K}_w(u, f))^- \|(\nabla_w^- f)(u)\|_\infty \\ f(u, 0) = f_0(u). \end{cases} \tag{13}$$

The time discretization leads to the following equation:

$$\begin{aligned} f^{n+1}(u) = & [1 - \Delta t |\mathcal{K}_w(u, f^n)|] f^n(u) + \\ & \Delta t (\mathcal{K}_w(u, f^n))^+ \cdot NLD(f^n)(u) + \\ & \Delta t (\mathcal{K}_w(u, f^n))^- \cdot NLE(f^n)(u), \end{aligned} \tag{14}$$

with:

$$\begin{aligned} NLD(f)(u) &= f(u) + \|(\nabla_w^+ f)(u)\|_\infty \\ NLE(f)(u) &= f(u) - \|(\nabla_w^- f)(u)\|_\infty. \end{aligned} \quad (15)$$

One can remark that this filter alternates between the non-local dilation of the image or non-local erosion of the image according to the sign of the curvature.

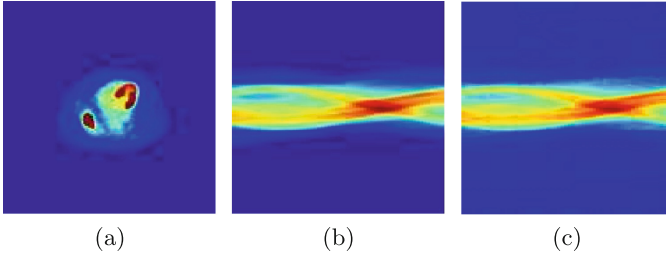


Fig. 1. Input image: (a) PET phantom used in simulation study (b) Noise-free sinogram (c) Noisy sinogram.

4 Results and Discussion

In this section, we compared the reconstruction results of the conventional ART algorithm, the proposed ART with local and nonlocal mean curvature flows filtering algorithm (ART-MCFL and ART-MCFNL) and Simultaneous algebraic reconstruction technique (SART) [14] for image reconstruction in PET.

4.1 Performance Evaluation

To evaluate the reconstructed results two criterions are calculated for the four implemented algorithms in addition to the visual quality of the resulting reconstructed images, in addition to the relative norm errors and the visual quality of the reconstructed image. The quality measurement is listed below:

The peak signal-to-noise ratio (PSNR) is defined as

$$PSNR = 10 \log \frac{255^2}{\frac{1}{MN} \sum_{j=1}^M \sum_{i=1}^N (x_{j,i} - x'_{j,i})^2} \quad (16)$$

The test image's grey level value is denoted by x , with x' being the same value as in the reconstructed image.

Abdomen image acquired on a PET scan was used in this study to simulate the few-view projection data (see Fig. 1(a)). To create a projection data, the simulated phantom image was forward projected using the system matrix to generate the noise-free projection data (Fig. 1(b-c)). Once the simulated noise-free sinograms were produced, a 30% uniform background was added to simulate mean randoms and scatters.

4.2 Experiments

The resultant reconstructed images obtained from conventional ART, ART-MCF and SART algorithms with 30 iterations, are shown in Fig. 2. From this Figure, the visual quality of the reconstructed image of the phantom using the ART-MCF algorithm is comparable to the other methods. As compared to some others methods, the experimental algorithm preserves edges better. The effectiveness of noise removal for the test algorithm was comparable to that of SART method; however, the intensity in the ROI was appreciably higher in the latter. Compared to the other methods, the ART-MCF method generates a superior intensity profile while preserving the edges.

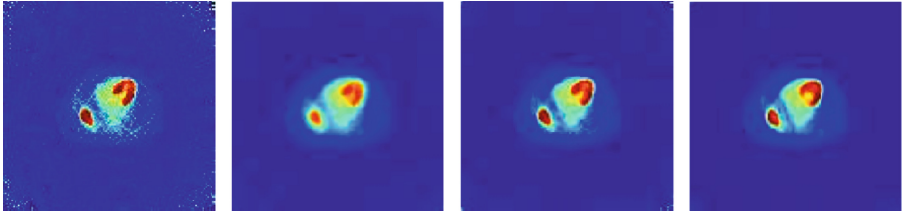


Fig. 2. Reconstructed images of the PET phantom by different algorithms. (a) ART ($PSNR = 19.25$), (b) SART ($PSNR = 30.35$), (c) ART-MCF local ($PSNR = 30.28$), (d) ART-MCF ($PSNR = 33.73$).

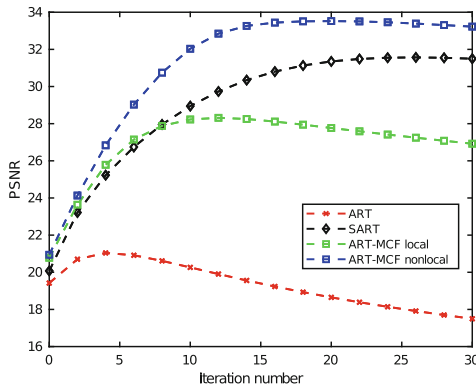


Fig. 3. PSNR vs iterations for ART, SART, and proposed methods.

The resultant of quality measurements ($PSNR$) of reconstructed images obtained from these algorithms by varying the number of iterations, are shown in Fig. 3. The later demonstrates that ART-MCF is providing better quality measurements than that of conventional ART and SART. The number of iterations is much required in order to enhance the image quality.

All the visual-displays, the quality measurement and the line plots suggest that the proposed ART-MCF algorithm is preferable to the other algorithms. From all the above observations, it may be concluded that the proposed algorithm is performing better in comparison to conventional algorithms and provide a better reconstructed image.

5 Conclusion

In this paper, we have adopted the PdE framework, and we have focused on some PDEs-based continuous morphological operators in the Euclidean domain: dilation/erosion and mean curvature flows. We have extended their applications for the processing of 2D PET images. We briefly presented the construction of a graph from 2D PET images and showed several examples, such as restoration, denoising or object extraction for medical purposes.

Acknowledgment. A. Emoataz is supported by the ANR SUMUM (ANR-17-CE38-0004).

References

1. Turkington, T.G.: Introduction to pet instrumentation. *J. Nucl. Med. Technol.* **29**(1), 4–11 (2001)
2. Hsieh, J., et al.: *Computed Tomography: Principles, Design, Artifacts, and Recent Advances*. SPIE, Bellingham (2009)
3. Fernandez, J.J.: Computational methods for electron tomography. *Micron* **43**(10), 1010–1030 (2012)
4. Natterer, F.: *The Mathematics of Computerized Tomography*. Siam, Philadelphia (1986)
5. Fessler, J.A.: Penalized weighted least-squares image reconstruction for positron emission tomography. *IEEE Trans. Med. Imaging* **13**(2), 290–300 (1994)
6. Anastasio, M.A., Zhang, J., Pan, X., Zou, Y., Ku, G., Wang, L.V.: Half-time image reconstruction in thermoacoustic tomography. *IEEE Trans. Med. Imaging* **24**(2), 199–210 (2005)
7. Boudjelal, A., Messali, Z., Elmoataz, A.: A novel kernel-based regularization technique for pet image reconstruction. *Technologies* **5**(2), 37 (2017)
8. Boudjelal, A., Messali, Z., Elmoataz, A., Attallah, B.: Improved simultaneous algebraic reconstruction technique algorithm for positron-emission tomography image reconstruction via minimizing the fast total variation. *J. Med. Imaging Radiat. Sci.* **48**(4), 385–393 (2017)
9. Dempster, A.P., Laird, N.M., Rubin, D.B.: Maximum likelihood from incomplete data via the EM algorithm. *J. Roy. Stat. Soc. B (Methodol.)* **39**, 1–38 (1977)
10. Shepp, L.A., Vardi, Y.: Maximum likelihood reconstruction for emission tomography. *IEEE Trans. Med. Imaging* **1**(2), 113–122 (1982)
11. Gordon, R., Bender, R., Herman, G.T.: Algebraic reconstruction techniques (ART) for three-dimensional electron microscopy and x-ray photography. *J. Theor. Biol.* **29**(3), 471–481 (1970)

12. Elmoataz, A., Lezoray, O., Bougleux, S.: Nonlocal discrete regularization on weighted graphs: a framework for image and manifold processing. *IEEE Tran. Image. Process.* **17**(7), 1047–1060 (2008)
13. Ta, V.T., Elmoataz, A., Lezoray, O.: Nonlocal PDEs-based morphology on weighted graphs for image and data processing. *IEEE Trans. Image. Process.* **26**(2), 1504–1516 (2011)
14. Andersen, A.H., Kak, A.C.: Simultaneous algebraic reconstruction technique (SART): a superior implementation of the ART algorithm. *Ultrason. Imaging* **6**(1), 81–94 (1984)